DATA REPOSITORY ITEMS

Stratigraphy and rifting age

The Lower sequence (0.6 km of inner-shelfal and dolomitic limestone) currently forms the sharp-rimmed morphology of the escarpment, while the Middle and Upper sequences have largely been eroded both out- and inboard of the escarpment as a result of shoulder uplift. Faults inboard of the main escarpment reflect post-Eocene displacements but are readily restored to their pre-rift geometries through balanced cross-sections based on geologic maps. Based on Roger et al. (1989), Platel and Roger (1989), Platel et al. (1992), Watchorn et al. (1998) and Fournier et al. (2004), the age of rifting is based stratigraphically on the 28–18 Ma age of syn-rift calci-turbitites (Mughsay Fm) contained in grabens. The existence locally of older (35–28 Ma) and fairly thin deposits, the base of which is lacustrine (Zalumah Fm), suggests an onset of crustal deformation and subaerial erosion of the top of the Eocene sequence soon after it was laid down. This may reflect the beginning of the rift phase, unless some « epeirogenic » movements caused by an elusive endogenous process preceded rifting and drove margin uplift. Surface uplift of the margin after 28 Ma certainly occurred because the calci-turbidites, which suggest paleobathymetries of > 500 m, are currently at outcrop level in southern Oman.

Low-temperature thermochronology: analytic procedure

Samples were collected following a fairly regularly spaced grid in order to avoid over- or under-sampling particular areas, and from the widest possible range of basement lithologies in order to increase chances of finding apatite. However, two samples, S2 and S3, contained no apatite, and large outcrops of low-grade metamorphic rock also lacked apatite. As a precaution to minimize the risk of diffusive He loss at surface temperatures in a hot climate (Trull et al., 1995), only the inner cores of cobble-sized samples were subjected to apatite extraction using conventional jaw-crushing, sieving, and heavy liquid and magnetic separation. Samples were irradiated at the well-thermalised (Cd ratio for Au >100) Hifar reactor, Lucas Heights, Australia, using the Corning CN5 glass dosimeter. Analyses were carried out on a Zeiss Axioplan microscope at a magnification of x1250, using a dry (x100)

objective. Confined track length measurements were made using a drawing tube and digitizing tablet, calibrated against a stage micrometer. Single-grain AFT ages were calculated using the external detector method and the zeta calibration approach, as recommended by the I.U.G.S. Subcommission on Geochronology (Hurford, 1990). Track length measurements were restricted to confined tracks parallel to the c-crystallographic axis.

Large (> 100 μm diameter), euhedral crystals were hand-picked under a stereomicroscope for (U–Th)/He dating. Grain populations were inspected at x700 magnification under cross-polarized light; selected when free of inclusions, fractures and other defects; further checked at higher magnifications for micro-inclusions; photographed; and loaded into platinum microtubes for helium outgassing and U/Th determination. Crystal prism dimensions were measured individually with a digitizing tablet. Absence of parent nuclide zoning in samples was ascertained from the fission-track distribution in crystal populations and their respective detectors used for AFT analysis. It was assumed that the Th distribution was equally uniform. Four of the apatite-yielding samples were unsuitable and therefore not used for (U–Th)/He dating. Samples were outgassed using an induction furnace at temperatures of 950 °C. The abundance of ^{4}He was measured relative to a 99.9% pure ^{3}He spike in a Pfeiffer Prisma 200 quadrupole mass spectrometer. For each crystal, the procedure was repeated to check for more tightly bound ^{4}He components trapped in undetected inclusions. If this re-extract failed to yield ^{4}He at levels higher than those detected by hot blanks, then the ^{4}He abundances (measured in counts / second, converted to ncc and corrected for blank) were deemed suitable for entering into the age equation. U and Th were analyzed in aqueous solution using an Agilent 7500 quadrupole mass spectrometer using spiked solutions of the dissolved apatite.

Although there currently exists no accepted standard manner of calculating statistical uncertainty around (U–Th)/He ages, these are reported here with analytical error. This includes errors on He, U and Th measurements and calibrations as well as ^{3}He, U and Th spikes. Repeated analysis of the California Institute of Technology Durango apatite standard reproducibility based on 39 analyses gives an age of 31.3±1.2 Ma (2 sigma). This error of the mean (6.7%), combined with the U/Th and He analytical uncertainties, is used

as a measure of the total uncertainty in sample age. Because each crystal potentially contains unique sources of uncertainty, a further key procedure consisted in measuring 2 to 4 replicates of the same sample. Although time consuming, this empirical approach is currently recognized as the most robust.

Low-temperature thermochronology: data modeling

Following the forward modeling procedure made available in HeFTy (Ketcham, 2005), fine tuning of thermal trajectories around the stratigraphically defined points of passage within the t–T space was achieved graphically by trial and error in order to obtain the best possible simultaneous fits between all of the following measured and model parameters: apatite central age, mean track length, standard deviation of track length distribution, replicate helium ages, as well as the visual quality of fit between the observed and model track-length distributions. Discordant (U–Th)/He single-grain ages (cf. Table DR2) were dealt with by focusing on the mean age of replicates. The goodness-of-fit (GOF) values between measured data and statistical moments predicted by the model were calculated using a Kuiper's test [a variant of the Kolmogorov-Smirnov (K-S) test, but equally sensitive in the tails and the median of a distribution]. In principle, a t–T path is supported by the data when the Kuiper's statistic value exceeds 0.50. Here, targets were set higher and considered to have been met when all GOF values (for AFT age, AFT track distribution, and ^{4}He grain ages) were simultaneously greater than 0.80, indicating excellent fits.

Dissimilarities between individual sample cooling histories within this small geographic region are likely to be partly due to kinetic parameters. For instance (Table DR1), a few samples fail the chi-2 test. However, Fig. DR1 helps to clarify the sources of error. Apart from sample S1 there is no systematic relationship between age and the kinetic parameter Dpar. Sample S1 does show some young ages lining up with smallest etch pits (suggesting zero to very low chlorine). Only three young grains, however, are driving this bias. Sample S7, for instance, only just fails the chi-2 test because of one older grain. Regarding the youngest sample, S6, the AFT and AHe ages (DR Tables 1 and 2) are close and suggest comparatively rapid cooling through the PAZ. Furthermore, sample S6 exhibits the youngest AFT age and may weakly confirm the spatial pattern inferred from the

stratigraphy. However, S6 also has the lowest number of measured track lengths (n = 58), so note that its apparent 'uniqueness' may be due to an oversampling of long tracks despite the clear presence of very short ones — also observed in all the other samples. This is a common source of uncertainty in AFT analysis. In summary, despite weak evidence for compositional overdispersion in sample S1, the other samples are behaving similarly in their response to annealing history. These observations mitigate any overdue sense of heterogeneity in the data set.

DR References

Fournier, M., Bellahsen, N., Fabbri, O., and Gunnell, Y., 2004, Oblique rifting and segmentation of the NE Gulf of Aden passive margin: Geochemistry, Geophysics, Geosystems, 5, Q11005, doi:10.1029/2004GC000731.

Hurford, A.J., 1990, Standardization of fission track dating calibration: recommendation by the Fission Track Working Group of the IUGS subcommission on geochronology. Chemical Geology, v. 80, p. 177–178.

Ketcham, R.A., 2005, Forward and inverse modeling of low-temperature thermochronometry data. Reviews in Mineralogy and Geochemistry, 58, 275–314.

Platel, J.-P., Roger, J., Peters, T.J., Mercolli, I., Kramers, J.D., and Le Métour, J., 1992, Geological map of Salalah, Sultanate of Oman, scale 1:250 000, sheet NE 40-09: Oman Ministry of Petroleum and Minerals, Directorate General of Mines.

Platel, J.-P., and J. Roger, 1989, Évolution géodynamique du Dhofar (Sultanat d'Oman) pendant le Crétacé et le Tertiaire en relation avec l'ouverture du golfe d'Aden. Bulletin de la Société Géologique de France, v. 2, p. 253–263.

Roger, J., Platel, J.-P., Cavelier, C., and Bourdillon-de-Grisac, C., 1989, Données nouvelles sur la stratigraphie et l'histoire géologique du Dhofar (Sultanat d'Oman): Bulletin de la Société Géologique de France, v. 2, p. 265–277.

Trull, T.W., Brown, E.T., Marty, B., Raisbeck, G.M., and Yiou, F., 1995, Cosmogenic ^{10}Be and ^{3}He accumulation in Pleistocene beach terraces in death valley, California, USA – implications for cosmic ray exposure dating of young surfaces in hot climates. Chemical Geology, v. 119, p. 191–207.

Watchorn, F., Nichols, G.J., and Bosence, D.W.J., 1998, Rift-related sedimentation and stratigraphy, southern Yemen (Gulf of Aden), *in* Purser, B.H., Bosence, D.W.J., eds., Sedimentation and tectonics of rift basins: Red Sea–Gulf of Aden: Chapman and Hall, London, p. 165–189.

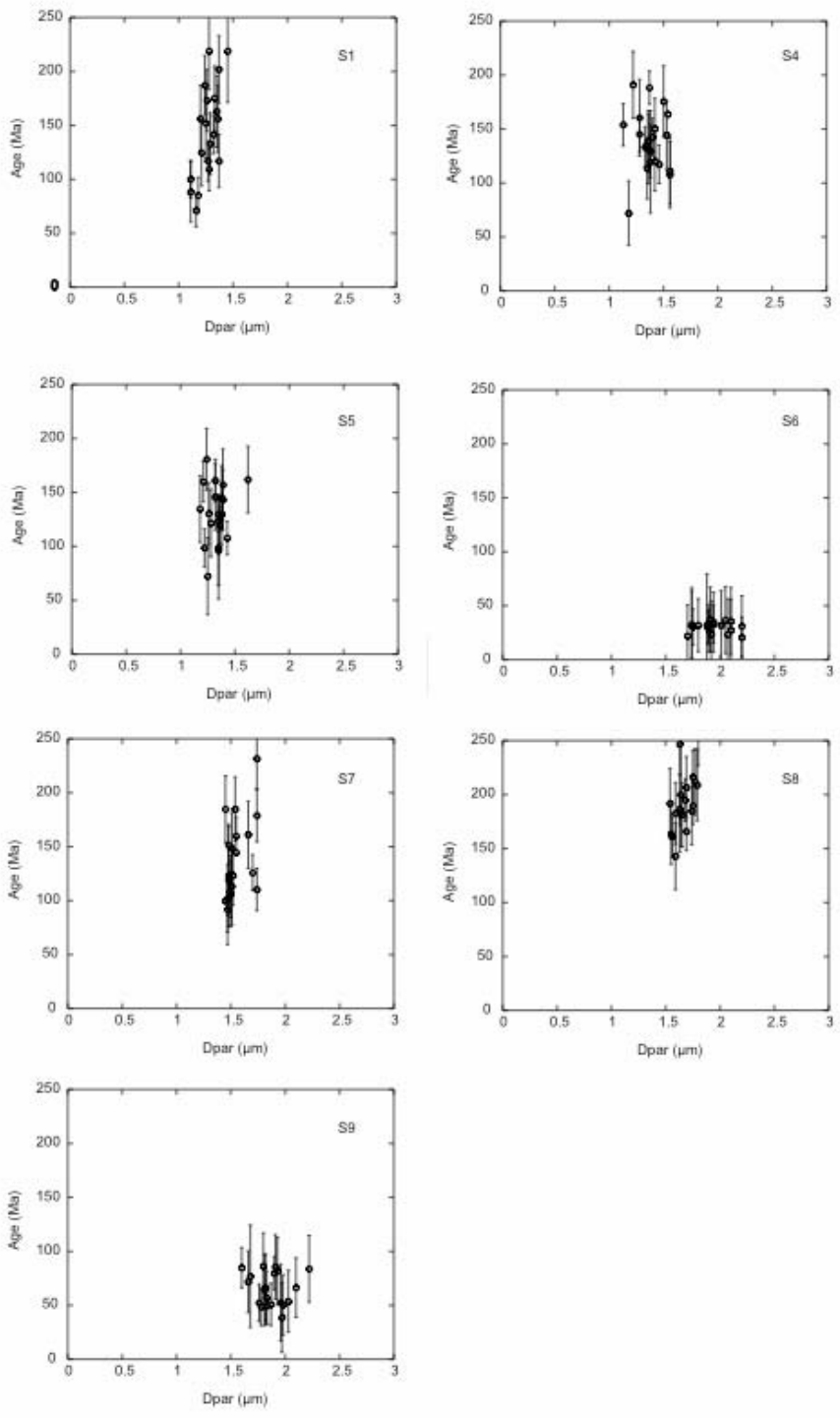

Fig. DR1. Plots of D_{par} vs. apparent age.

TABLE DR1. APATITE FISSION-TRACK DATA FOR S. DHOFAR (OMAN)

Sample name	No. of crystals	Dosimeter*		Spontaneous*		Induced*		Age dispersion		Central age§	Mean track length	S.D.	No. of tracks
		ρ_d	N_d	ρ_s	N_s	ρ_i	N_i	$P\chi^2$†	RE	(Ma ± 1σ)	(μm)	(μm)	
S1	20	1.317	3651	0.789	1029	1.22	1589	0	24.0	141.0±9.8	10.57±0.26	2.33	75
S4	22	1.317	3651	0.626	1161	1.015	1338	36	5.9	136.1±5.9	11.88±0.14	1.46	102
S5	20	1.317	3651	1.274	1638	2.237	2667	0.9	11.7	132.2±6.0	12.11±0.17	1.74	75
S6	20	1.317	3651	0.689	808	4.917	5765	80	0	31.1±1.3	13.28±0.24	1.87	58
S7	20	1.317	3651	1.340	2139	1.503	2396	1.5	10.9	195.6±8.3	11.46±0.17	1.69	100
S8	22	1.317	3651	0.561	701	0.948	902	51	0.8	130.4±6.6	11.23±0.21	2.12	101
S9	20	1.317	3651	1.364	1835	4.68	6292	0	19.6	64.4±3.5	11.49±0.29	2.87	100

Note: Analyses by external detector method using 0.5 for the $4\pi/2\pi$ geometry correction factor. Ages calculated using dosimeter glass CN-5 and ζ (zeta) calibration procedure; ζ_{CN5} = 339 ± 4, calibrated by multiple analyses of IUGS apatite and zircon age standards.

*Track densities are ($x10^6$ tr·cm^{-2}) numbers of tracks counted (N).

†$P\chi^2$ is probability for obtaining χ^2 value for n degrees of freedom, where n = No. crystals – 1.

§Central age is a modal age, weighted for different precisions of individual crystals.

TABLE DR 2. (U–TH)/HE REPLICATE ANALYSES (S. DHOFAR, OMAN)

Sample name	^{4}He	^{238}U	^{232}Th	Grain Radius	Grain Length	Uncorrected age	Error ±7%
	(ncc)	(ng)	(ng)	(μm)	(μm)	(Ma)	
S4-1	0.691	0.19	0.08	165	228	26.8	1.87
S4-3	0.315	0.11	0.09	109	288	19.0	1.32
S4-4	0.273	0.09	0.11	110	202	18.5	1.29
S6-1	0.763	0.19	0.21	107	240	25.9	1.81
S6-2	0.983	0.22	0.25	112	250	28.2	1.97
S6-4	1.317	0.30	0.31	87	240	28.2	1.97
S9-1	1.808	0.46	0.33	115	240	27.6	1.93
S9-3	2.016	0.40	0.47	102	254	32.3	2.26
S9-4	0.732	0.22	0.18	106	274	22.4	1.56